nature materials

LETTERS

PUBLISHED ONLINE: 20 NOVEMBER 2011 | DOI: 10.1038/NMAT3178

Self-assembly of uniform polyhedral silver nanocrystals into densest packings and exotic superlattices

Joel Henzie[1], Michael Grünwald[1]*, Asaph Widmer-Cooper[1,2,3], Phillip L. Geissler[1,2] and Peidong Yang[1,2,4]*

Understanding how polyhedra pack into extended arrangements is integral to the design and discovery of crystalline materials at all length scales[1–3]. Much progress has been made in enumerating and characterizing the packing of polyhedral shapes[4–6], and the self-assembly of polyhedral nanocrystals into ordered superstructures[7–9]. However, directing the self-assembly of polyhedral nanocrystals into densest packings requires precise control of particle shape[10], polydispersity[11], interactions and driving forces[12]. Here we show with experiment and computer simulation that a range of nanoscale Ag polyhedra can self-assemble into their conjectured densest packings[6]. When passivated with adsorbing polymer, the polyhedra behave as quasi-hard particles and assemble into millimetre-sized three-dimensional supercrystals by sedimentation. We also show, by inducing depletion attraction through excess polymer in solution, that octahedra form an exotic superstructure with complex helical motifs rather than the densest Minkowski lattice[13]. Such large-scale Ag supercrystals may facilitate the design of scalable three-dimensional plasmonic metamaterials for sensing[14,15], nanophotonics[16] and photocatalysis[17].

New synthetic methods give access to a wide range of well-defined polyhedral nanocrystalline shapes. The polyol synthesis was used to generate monodisperse Ag nanocrystals (Supplementary Methods) including cubes, truncated cubes, cuboctahedra, truncated octahedra and octahedra over a range of sizes from 100 to 300 nm (Fig. 1a; refs 7,18). These Ag nanocrystals are coated with polyvinylpyrrolidone (PVP; relative molecular mass 55,000), which enables the shape-controlled synthesis and acts as a stabilizer[19]. Of these five shapes, only cubes and truncated octahedra possess space-filling packings. For the other three shapes, as for most non-spherical shapes, no rigorous statements about optimal packings exist. For any convex shape, however, the densest lattice packing can be calculated explicitly[4,13]. Lattice packings are a special class of arrangements in which all particles are oriented identically and positioned at sites of a crystalline lattice. Whereas it is generally not true that the densest lattice packing constitutes the overall densest packing for a given shape, a recent conjecture indicates that the centrally symmetric Platonic and Archimedean solids—families of convex polyhedra that include the shapes studied here but, notably, do not include tetrahedra—pack most densely into these lattice packings[6]. Yet this statement does not guarantee that such structures are thermodynamically stable at finite pressure, nor that they can be readily accessed through random thermal motion. Indeed, computer simulations show, in the related case of tetrahedra, that these factors result in self-assembly of an intriguing quasicrystal that is not the densest packing[5,20–22].

In our experiments, monodisperse Ag polyhedra assemble into large ($>25\,mm^2$), dense supercrystals by gravitational sedimentation (Fig. 1b). This process can be carried out in bulk solution, but assembly in polydimethylsiloxane (PDMS) reservoirs (Supplementary Methods) enables precise control of the superlattice dimensions and monitoring by dark-field optical microscopy (Fig. 1c). *N*, *N*-dimethylformamide (DMF) was used as the assembly medium because it is an excellent solvent for PVP. In a typical experiment, a dilute solution of particles was loaded into the reservoir so that the channel filled with a uniform solution of particles (Supplementary Methods). Then the device was tilted, causing the particles to gradually sediment and assemble at the bottom of the reservoir (Fig. 1c and Supplementary Movies S1–S3); more concentrated solutions or higher angles of tilt cause the assemblies to form more quickly.

The assemblies generated by this sedimentation procedure, shown in Fig. 1d–h, exhibit translational and rotational order over exceptional length scales, as illustrated in Fig. 2a–d. In the cases of cubes, truncated octahedra and octahedra, the structures of the dense supercrystals correspond precisely to their densest lattice packings. The same packings are observed to form in constant-pressure Monte Carlo simulations (Supplementary Methods) of dense fluids of hard polyhedra (Supplementary Figs S2, S5 and Movie S4). Ag cubes (Fig. 1d) form dense arrangements that fill space. In small assemblies, cubes tend to occupy the sites of a simple cubic lattice and form supercubes of up to 10 μm edge length. In larger assemblies the symmetry of the simple cubic lattice is broken and more irregular, space-filling packings are observed. Truncated octahedra assemble into the space-filling Kelvin structure (Fig. 1g), which corresponds to the body centred cubic lattice. Of all the shapes studied here, assemblies of truncated octahedra exhibit single-crystalline order over the largest length scales. Ag octahedra (Fig. 1h) assemble into a packing that was recognized long ago by Minkowski as the densest lattice packing for this shape[13]. Unlike cubes and truncated octahedra, octahedra in their densest lattice packing engage in only incomplete face-to-face contact; equivalent faces of neighbouring octahedra also do not lie in a common plane. As discussed later, these features enable simple biases to stabilize alternative packings. In Fig. 2f, a rendering of the perfect Minkowski lattice is superimposed on the experimental lattice,

[1]Department of Chemistry, University of California, Berkeley, California 94720, USA, [2]Materials Sciences Division, Lawrence Berkeley National Laboratory, Berkeley, California 94720, USA, [3]School of Chemistry, University of Sydney, Sydney, New South Wales 2006, Australia, [4]Department of Materials Science and Engineering, University of California, Berkeley, California 94720, USA. *e-mail: michael.gruenwald@berkeley.edu; p_yang@berkeley.edu.

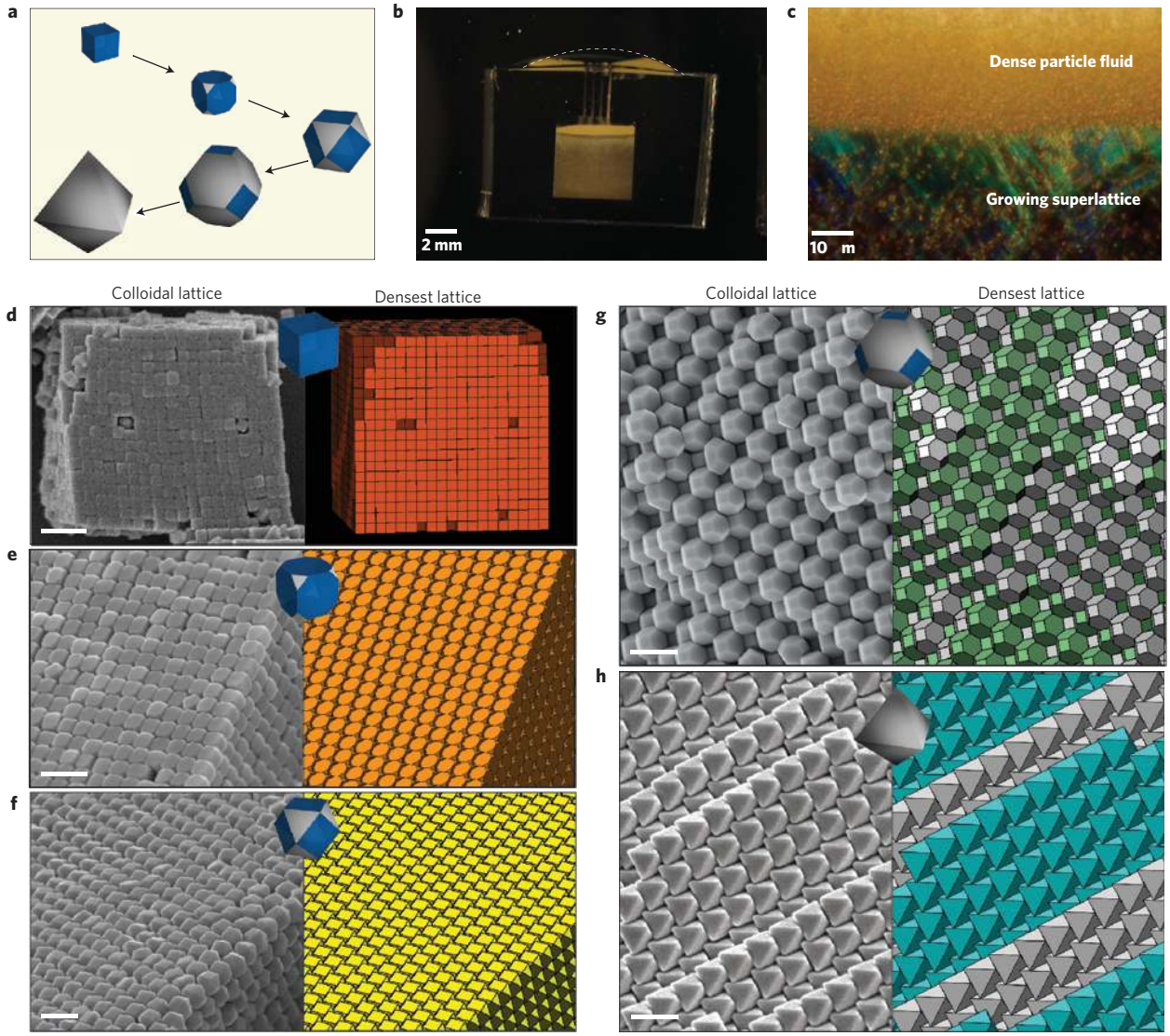

Figure 1 | Self-assembly of dense polyhedron lattices. a, Schematic representation of polyhedral shapes accessible using the Ag polyol synthesis. **b**, Microfluidic reservoir used to assemble the Ag nanocrystals. **c**, Dark-field micrograph showing the growing Ag supercrystal. **d**–**h**, SEM micrographs of the colloidal lattices (left) and the corresponding diagrams of their densest known lattice packings (right): **d**, cubes; **e**, truncated cubes; **f**, cuboctahedra; **g**, truncated octahedra; **h**, octahedra. Colour in **g** and **h** is used to indicate different layers of the crystal. Scale bars are 500 nm unless otherwise noted.

showing excellent agreement. A detailed comparison of Fourier patterns is shown in Supplementary Fig. S1.

Cuboctahedron and truncated cube Ag nanocrystals also adopt very dense, ordered structures that closely resemble their densest lattice packings (Fig. 1e,f). For truncated cubes, the densest packing is only subtly different from the simple cubic lattice and their packing fractions differ by only 0.7%. We therefore expect that high pressures are necessary to bias the assembly towards the densest packing. In our experiments, truncated cubes form lattices that vary from almost perfect cubic alignment to the characteristic tilt of the densest packing. Monte Carlo simulations of truncated cubes similarly exhibit variability at moderate, experimentally accessible pressures. In fact, even at very high pressures the densest packing was never observed to form spontaneously from the fluid on the timescale accessible to straightforward simulation. By contrast, simulations of hard cuboctahedra readily achieve the densest lattice packing at moderately high pressures whereas experimentally assembled lattices vary between the densest packing and a slightly distorted lattice with face-centred-cubic-like symmetry (Supplementary Fig. S3).

Calculations confirm that gravity is indeed a plausible driving force in our assembly experiments. Unlike smaller nanocrystals used in conventional, evaporation-driven assembly studies, our Ag particles are 100–300 nm in size and experience substantial gravitational forces, for octahedra amounting to 0.23 $k_B T$ per micrometre. To estimate the pressures that develop within the sediment, we carried out Monte Carlo simulations of octahedra under the influence of gravity (Supplementary Methods), in an elongated box with a hard bottom wall (Fig. 3a). To mimic the experimental set-up, simulations were started at uniform low density, enabling the particles to sediment, eventually achieving a density gradient approximately 150 μm in height. Resulting pressures near the bottom of the model cell were sufficient for spontaneous crystallization into the Minkowski lattice. Experimental sedimentation channels feature even higher columns of dense material, and therefore pressures more than sufficient to drive crystallization. Further evidence comes from experimental waiting times. Whereas the larger octahedra (300 nm edge length, 1.33×10^{-13} g) sediment within a few hours, the smaller cubes (122 nm edge length, 1.90×10^{-14} g) take significantly longer to assemble.

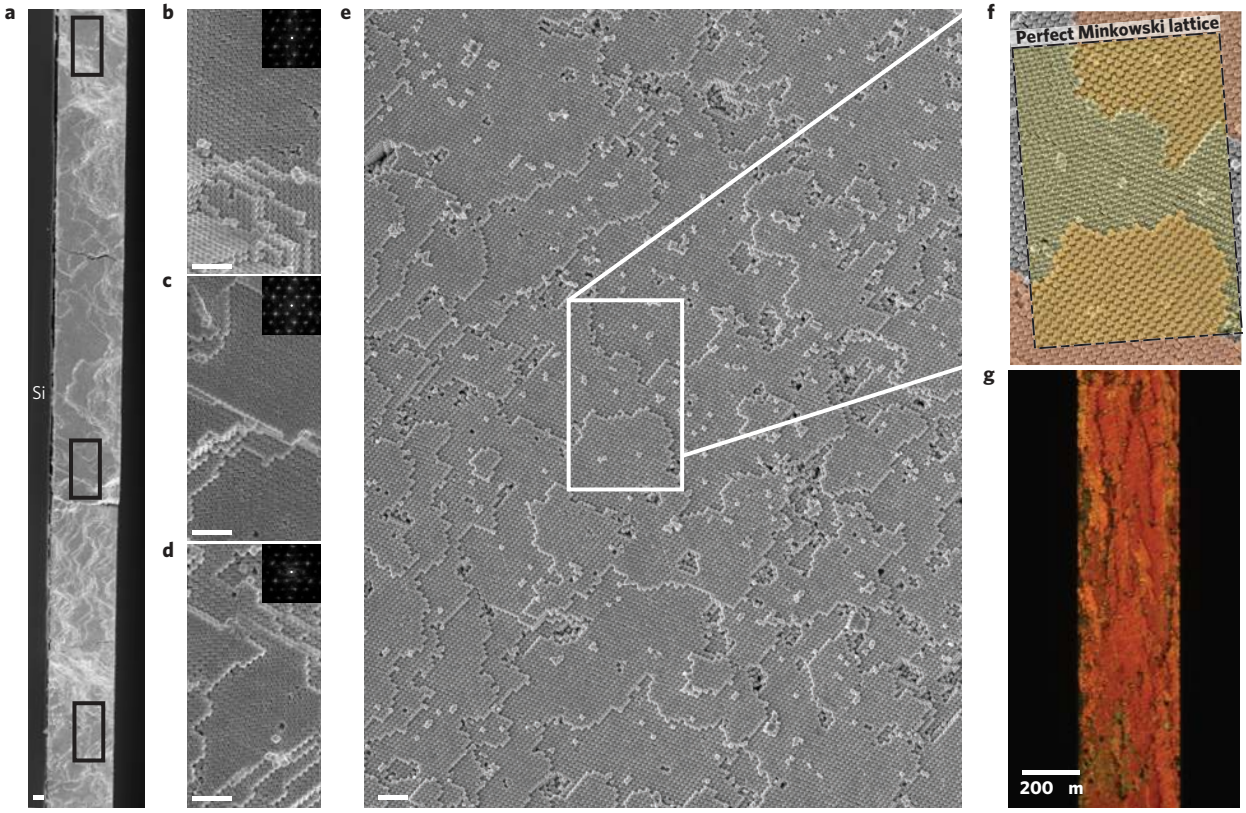

Figure 2 | Long-range order of assembled lattices. Large-scale SEM images of an octahedron lattice on a Si substrate. **a**, The imaged region is a cross-section of a large supercrystal that extends millimetres below the plane of the image, and was exposed by cleaving the substrate and superlattice into two pieces. **b–d**, Inspection of particle orientation in the magnified sections reveals that long-range order is maintained across the entire imaged sample. Insets: Fourier transforms of these sections match closely. **e**, SEM image of a large Minkowski facet. **f**, A magnified section of the experimental lattice with a superimposed rendering of the ideal Minkowski lattice shows excellent agreement. **g**, Cross-polarized optical micrograph of a millimetre-sized superlattice slab. The uniform colour of the reflected light from top to bottom indicates that the crystal is composed of a single domain. All scale bars are 2 μm unless otherwise noted.

Both in experiment and simulation, octahedra packed against a flat substrate form a structure that is different from but closely related to the Minkowski lattice (Fig. 3c–e). This simple hexagonal lattice has a maximum packing fraction of 8/9 and is composed of flat, hexagonally close-packed layers that stack with perfect face-to-face contact between the layers (Fig. 3e). Octahedra in the corresponding layers of the Minkowski lattice (Fig. 3f, right) are slightly rotated, which results in increased packing efficiency (18/19) through interpenetration of stacked layers. In the presence of a flat wall, however, local packing efficiency is maximized by flattening the layers. This boundary effect extends only a short distance into the sample. In both experiment and simulation, the simple hexagonal packing type gives way to the Minkowski structure after a few close-packed layers.

That structures determined by shape and high pressure can be achieved in our self-assembly experiments indicates that particles are behaving as almost purely hard, non-attractive polyhedra. This conclusion is surprising, given the potentially overwhelming van der Waals (vdW) attractions between metallic objects of this size. At nanometre separations, the corresponding potential energy reaches tens of thousands of k_BT. If further repulsive forces did not preclude such separations, experiments would result in rapid aggregation of disordered, irreversibly bound particle aggregates. By contrast, assemblies are quite reversible before the drying step. When the assembly experiment is turned upside down, most of the assembled lattice dissociates and the nanocrystals begin to assemble at the 'new' bottom of the set-up (Supplementary Fig. S8). Significant electrostatic repulsion is unlikely because the measured zeta potential of the particles in DMF is close to zero (Supplementary Methods). Instead, experimental and computational evidence strongly suggests that the repulsion originates from the volume exclusion of the adsorbing polymer PVP.

Measurements of the hydrodynamic diameter of cuboctahedra with adsorbed polymer indicate that particles are covered with a PVP layer that extends 20 nm from the particle surface, which is roughly equal to the hydrodynamic diameter of free PVP in DMF (Supplementary Methods). Our calculations suggest that polymer layers of this thickness are sufficient to prevent close approach of nanocrystal surfaces. Figure 4a shows model predictions of different contributions to the interaction between two Ag octahedra, aligned face to face, as a function of their separation (Supplementary Fig. S6). The particles are assumed to be covered with a 20-nm-thick layer of dense polymer. As the polymer layers of the two octahedra come into contact, strong entropic repulsion competes with the vdW attraction of the Ag cores. The combined potential of mean force shows that the polymer-mediated repulsion is indeed sufficient to balance the vdW forces, resulting in a shallow effective energy minimum on contact between the surface polymer layers. To test the influence of the size of the adsorbed polymer brush on this force balance, we have repeated assembly experiments with ethanol and water as solvents. Measurements of the hydrodynamic diameter of cuboctahedra suggest brush thicknesses of roughly 15 nm in ethanol and 5 nm in water (Supplementary Methods). Calculations show that, on contact of the polymer brushes of two octahedra, the vdW energies amount to roughly $-14\,k_BT$ in ethanol

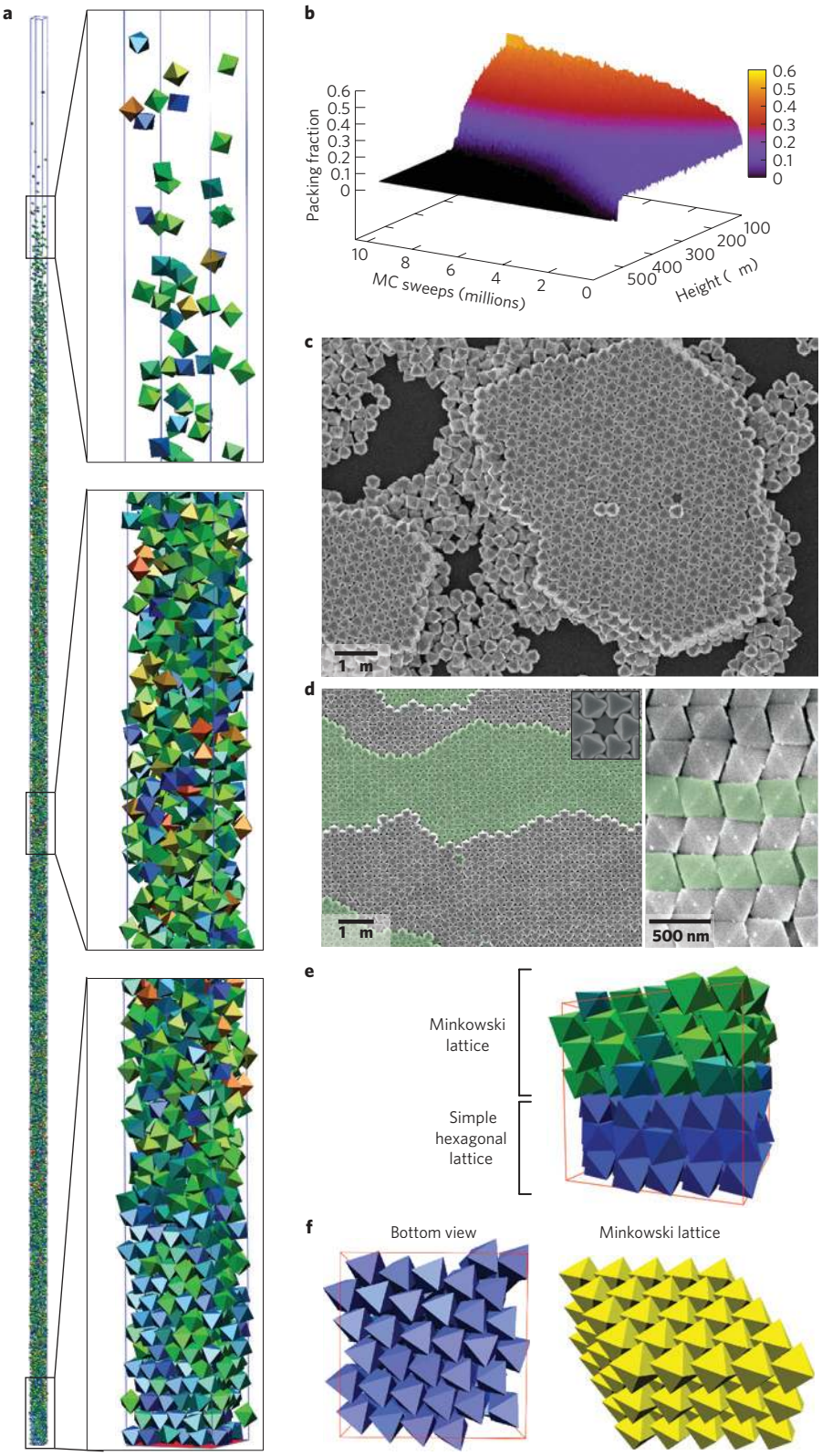

Figure 3 | Gravitational driving force and packings near surfaces. a, Snapshot of a Monte Carlo simulation (Supplementary Methods) of hard octahedra under the influence of gravity (left). Zoom-in images (right), from top to bottom, show a dilute fluid, a dense fluid and a growing solid of the Minkowski type. Octahedra are coloured according to orientation. **b**, Packing fraction as a function of Monte Carlo sweeps and height along the *z* axis in the elongated box. A density gradient develops in the initially homogenous system, resulting in a fluid–solid transformation at the bottom. Biased by a flat surface, octahedra form a simple hexagonal lattice (space group *P*6/*mmm*). **c**, Small patches of this structure, retrieved early in the assembly process. **d**, Top-down view (left), with inset showing a vacancy in the lattice, and side view (right). **e**, Zero-gravity, isobaric Monte Carlo simulations with a hard bottom wall and weak interparticle attractions show coexistence between the layered structure and the Minkowski lattice, consistent with experiment. **f**, Comparison between a flat layer of the simple hexagonal lattice (left) and corresponding staggered layers in the Minkowski lattice (right).

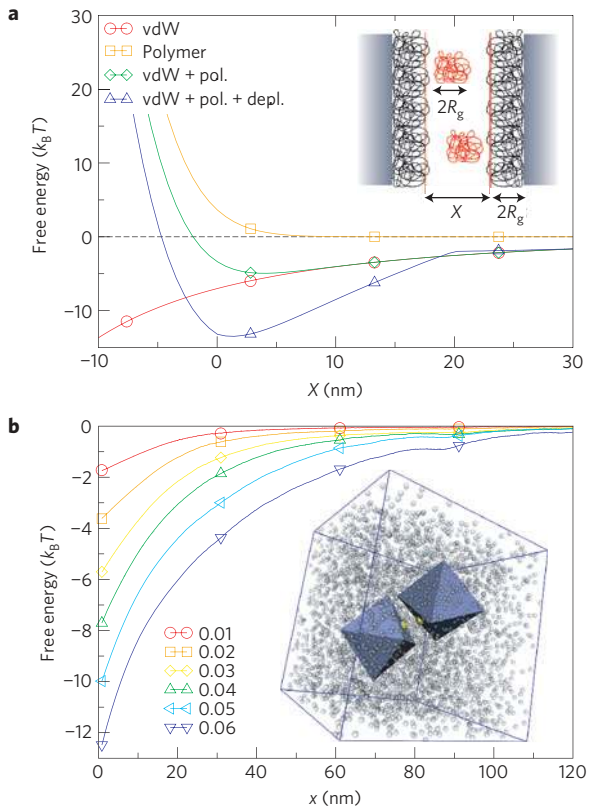

Figure 4 | Polymer-mediated nanocrystal interactions. a, Contributions to the free energy of two octahedra aligned face to face, as a function of the separation X of surface-adsorbed polymer layers (see inset; Supplementary Methods). The entropic repulsion (orange) of densely packed surface polymers (radius of gyration, Rg = 10 nm) dominates the vdW attraction (red) of the silver cores. The resulting potential (green) is only weakly attractive, enabling the nanocrystals to behave as quasi-hard particles. Unadsorbed polymer coils act as depleting agents, inducing effective attractions (blue) that can lead to self-assembly of different structures. **b**, Potentials of mean force for two hard octahedra in a bath of hard 20 nm spheres (see inset), as a function of the distance x between nearest midpoints of octahedron faces (see inset, interaction centres are marked in yellow), averaged over all rotational degrees of freedom. Legend values correspond to the sphere packing fraction φ.

and $-140\,k_BT$ in water (compare with $-7\,k_BT$ in DMF). The results of assembly experiments in these solvents are consistent with the estimated increasing attraction strengths: whereas we do observe some assembly of the Minkowski lattice in ethanol, albeit of inferior quality, we observe primarily disordered aggregation in water.

The effect of the residual vdW attractions is visible in many aspects of the assembly experiments: optical microscopy shows that particles can temporarily bind even at moderate concentrations (Supplementary Movie S1). Moreover, as discussed earlier in the text, cubes and truncated cubes show a preference for face-to-face alignment in small assemblies, as do close-packed octahedron layers near substrates. However, under conditions of high density, these weak, slowly varying attractive forces play a secondary role[23]. The nanocrystals behave essentially as hard particles with polyhedral shapes that are not modified or masked by the thin layer of adsorbed PVP. Nevertheless, the final dried assemblies shown in Fig. 1 are quite stable, with interparticle spacings of only a few nanometres. Surface polymer molecules, driven by high pressures and decreasing solvent concentration, evidently collapse or desorb at later stages of the experiments, enabling particles to approach closely and attract strongly (Supplementary Fig. S4).

Unadsorbed polymer in solution can also induce attractions between particles[24]. These depletion attractions are entropic forces generic to solutions of differently sized particles: at small separations, two of the larger particles exclude smaller ones from the intervening volume[25–27]. The resulting gradient in osmotic pressure (due to the gradient of density of the smaller species) induces an attraction between the large particles that increases with the bulk concentration of the smaller species. In our case, free polymer coils in solution act as depleting agents and mediate substantial attractions between polymer-coated nanocrystals: Fig. 4b shows effective pair potentials of hard octahedra in a bath of hard spheres, mimicking free polymer coils in solution, for several different volume fractions φ of the spheres (Supplementary Methods). Note that the typical oscillatory behaviour of depletion forces is not evident in these potentials, because they are averaged over all rotational degrees of freedom and polymer concentrations are low.

Experiments and simulations indicate that these tunable attractions can induce structures that are not governed solely by packing efficiency of hard shapes. Figure 5a,b shows scanning electron microscopy (SEM) micrographs of a lattice of octahedra with intriguing helical motifs that was generated by adding 0.1 μg μl^{-1} (w/v) of extra PVP to the solution immediately before sedimentation. Higher amounts of PVP resulted in less Minkowski lattice and more helical lattice. The large degree of face-to-face contact in the latter reflects significant attractive forces. The same structure was recovered in Monte Carlo simulations employing the effective depletion pair potentials shown in Fig. 4b, for $\varphi > 0.02$. (Further evidence for the stability of the helical structure in the presence of depleting agents is discussed in Supplementary Methods and Fig. S7.) Symmetry analysis of an optimized unit cell revealed that the structure has space group $I\bar{4}3d$, with a cubic unit cell containing 16 octahedra (Fig. 5d,e and Supplementary Section S1). Particle centres are located on 16c Wyckoff sites, similar to a high-pressure phase of lithium[28]; vertices occupy 48e sites. The maximal packing fraction of this structure (~82%) is significantly lower than that of the Minkowski lattice (~95%). This helical structure may also be more suitable as a plasmonic bandgap crystal because the lines and helices should create continuous transmission pathways with lower attenuation[7].

The approach we have used in this study circumvents several issues that have been a challenge for reproducible and tunable assembly of nanocrystal patterns over device-length scales. In many experiments the evaporation of solvent triggers organization of nanocrystal solutes. Such drying-mediated assembly can be difficult to control owing to the severity of solvation forces and their spatially non-uniform fluctuations[29]. In fact, we have tried several experimental geometries where solvent evaporation is a major driving force. In the simplest examples, a drop of nanocrystals in DMF was mounted on a substrate and evaporated in air, or placed in an atmosphere saturated with DMF vapour to slow evaporation. Whereas we observe the same types of crystal in these experiments, the degree of long-range order is inferior when compared with the samples obtained from sedimentation. Our observations indicate that gradual sedimentation, compared to solvent evaporation, provides a driving force that is gentle and homogeneous. Whereas sedimentation-driven assembly is not new, this is the first time that it has been used to make large-scale assemblies of polyhedral particles. In other approaches, anisotropic forces between particles primarily determine the structure of assembled patterns[10]. The key factor in our experiments is particle shape—a feature we have found easier to control. Depletion attractions are a secondary bias that can be easily tuned by adjusting the depleting agents' size and concentration. For octahedra this changes the packing from the Minkowski lattice to a less dense structure with more face-to-face contact.

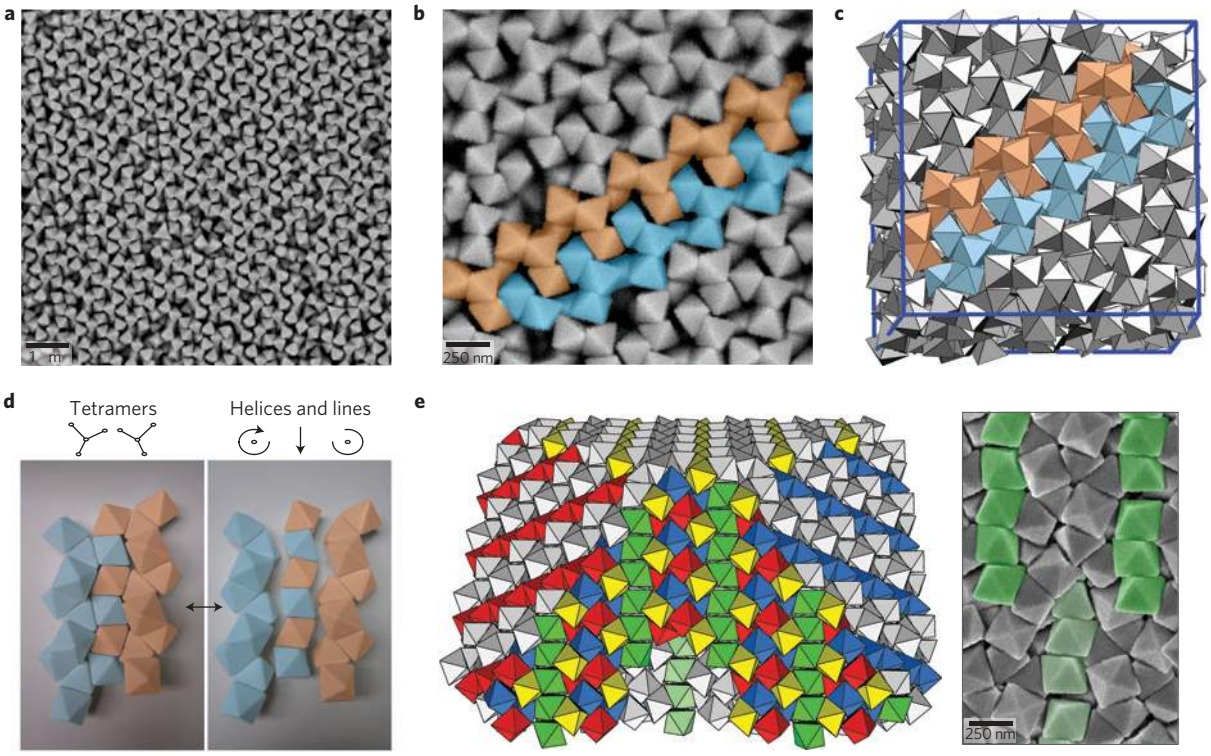

Figure 5 | Ag octahedra assemble into a previously unknown lattice in the presence of excess PVP. a, SEM micrograph of a new octahedron supercrystal. **b**,**c**, The lattice consists of tetramer motifs (**b**) and forms spontaneously in Monte Carlo simulations of octahedra with depletion attractions (**c**). **d**, The tetramers can be decomposed into lines and counter-rotating helices, where the helices in this plane consist of particles belonging to three other sets of interlocking lines. **e**, The lattice has been coloured to show these four equivalent sets of lines (yellow, blue, green and red) that are oriented in different [111] directions. Lines belonging to the same [111] direction are parallel and shifted relative to one another in alternating layers (green particles on left; right, enlarged SEM micrograph from the corresponding experimental lattice). When viewed end on (yellow particles), the particle lines stack hexagonally.

Simulations of attractive cuboctahedra also indicate that depletion attractions may be involved in the formation of the FCC-like structure observed experimentally (Supplementary Fig. S3). Other polyhedral shapes that pack densely with limited face-to-face contact may be similarly prone to switching structures under the addition of excess polymer. Polyhedral nanocrystals can be made from a variety of materials, including metals, dielectrics and semiconductors[30]. When compared with crystal structures of nearly spherical particles, dense packings of polyhedra are characterized by higher packing fractions, large interfaces between particles and different geometries of voids and gaps, which determine the electrical and optical properties of these materials[31,32]. The assembly procedures described here may thus give access to a wide range of interesting, scalable nanostructured materials with dimensions that are comparable to those of bulk materials.

Methods

Ag polyhedra were synthesized using methods described in refs 7,18 and were exceptionally monodisperse in both size and shape. The particles were suspended in DMF and loaded on top of a PDMS reservoir that had been filled with neat DMF. The entire set-up was placed in a weighing bottle to minimize solvent evaporation, and particles settled to the bottom of the PDMS chamber by gravity, assembling into nanocrystal superlattices. Measurements of hydrodynamic diameter and zeta potential were obtained using commercial light-scattering instrumentation (Zetasizer Nano, Malvern Instruments). The vdW potential was calculated from a coarse-grained atomistic representation of the octahedra, with 666,700 interaction sites per particle. For the calculation of the repulsion between polymer-covered surfaces, we assumed a dense packing of 100 spherical polymer coils per surface. Every adsorbed coil interacts with its counterpart on the opposing surface through a Gaussian core potential[33]. Effective pair potentials $w_\varphi(x)$ for octahedra in the presence of excess PVP were calculated according to $\beta w_\varphi(x) = -\ln P_\varphi(x)/P_{\varphi=0}(x)$. Here, $P_\varphi(x)$ is the distribution function of the distance x between nearest faces of octahedra in a bath of hard spheres with packing fraction φ, and $\beta = 1/k_B T$.

Received 11 March 2011; accepted 20 October 2011; published online 20 November 2011

References

1. Wells, A. F. *Structural Inorganic Chemistry* (Oxford Univ. Press, 1984).
2. O'Keeffe, M. & Hyde, B. G. *Crystal Structures I. Patterns and Symmetry* (Mineralogical Society of America, 1996).
3. Murray, C. B., Kagan, C. R. & Bawendi, M. G. Synthesis and characterization of monodisperse nanocrystals and close-packed nanocrystal assemblies. *Annu. Rev. Mater. Sci.* **30,** 545–610 (2000).
4. Betke, U. Densest lattice packings of 3-polytopes. *Comput. Geom.* **16,** 157–186 (2000).
5. Haji-Akbari, A. *et al.* Disordered, quasicrystalline and crystalline phases of densely packed tetrahedra. *Nature* **462,** 773–777 (2009).
6. Torquato, S. & Jiao, Y. Dense packings of the Platonic and Archimedean solids. *Nature* **460,** 876–879 (2009).
7. Tao, A. R., Ceperley, D. P., Sinsermsuksakul, P., Neureuther, A. R. & Yang, P. Self-organized silver nanoparticles for three-dimensional plasmonic crystals. *Nano Lett.* **8,** 4033–4038 (2008).
8. Xie, S. *et al.* Supercrystals from crystallization of octahedral MnO nanocrystals. *J. Phys. Chem. C* **113,** 19107–19111 (2009).
9. Quan, Z. & Fang, J. Superlattices with non-spherical building blocks. *Nano Today* **5,** 390–411 (2010).
10. Glotzer, S. C. & Solomon, M. S. Anisotropy of building blocks and their assembly into complex structures. *Nature Mater.* **6,** 557 (2007).
11. Auer, S. & Frenkel, D. Suppression of crystal nucleation in polydisperse colloids due to increase of the surface free energy. *Nature* **413,** 711–713 (2001).
12. Bishop, K. J. M., Wilmer, C. E., Soh, S. & Grzybowski, B. A. Nanoscale forces and their uses in self-assembly. *Small* **5,** 1600–1630 (2009).
13. Minkowski, H. Dichteste gitterförmige Lagerung kongruenter Körper. *Nachr. Akad. Wiss. Göttingen Math.-Phys.* **Kl. II,** 311–355 (1904).
14. Kabashin, A. V. *et al.* Plasmonic nanorod metamaterials for biosensing. *Nature Mater.* **8,** 867–871 (2009).
15. Novo, C., Funston, A. M. & Mulvaney, P. Direct observation of chemical reactions on single gold nanocrystals using surface plasmon spectroscopy. *Nature Nanotech.* **3,** 598–602 (2008).

16. Pendry, J. B., Schurig, D. & Smith, D. R. Controlling electromagnetic fields. *Science* **312,** 1780–1782 (2006).
17. Hung, W. H., Aykol, M., Valley, D., Hou, W. & Cronin, S. B. Plasmon resonant enhancement of carbon monoxide catalysis. *Nano Lett.* **10,** 1314–8 (2010).
18. Tao, A., Sinsermsuksakul, P. & Yang, P. Polyhedral silver nanocrystals with distinct scattering signatures. *Angew. Chem. Int. Ed.* **45,** 4597–4601 (2006).
19. Sun, Y. & Xia, Y. Shape-controlled synthesis of gold and silver nanoparticles. *Science* **298,** 2176–2179 (2002).
20. Chen, E. R., Engel, M. & Glotzer, S. C. Dense crystalline dimer packings of regular tetrahedra. *Discrete Comput. Geom.* **44,** 253–280 (2010).
21. Kallus, Y., Elser, V. & Gravel, S. Dense periodic packings of tetrahedra with small repeating units. *Discrete Comput. Geom.* **44,** 245–252 (2010).
22. Torquato, S. & Jiao, Y. Exact constructions of a family of dense periodic packings of tetrahedra. *Phys. Rev. E* **81,** 041310 (2010).
23. Weeks, J. D., Chandler, D. & Andersen, H. C. Role of repulsive forces in determining the equilibrium structure of simple liquids. *J. Chem. Phys.* **54,** 5237–5247 (1971).
24. Ruths, M., Yoshizawa, H., Fetters, L. J. & Israelachvili, J. N. Depletion attraction versus steric repulsion in a system of weakly adsorbing polymers—effects of concentration and adsorption conditions. *Macromolecules* **29,** 7193–7203 (1996).
25. Asakura, S. & Oosawa, F. Interaction between particles suspended in solutions of macromolecules. *J. Polym. Sci.* **33,** 183–192 (1958).
26. Baranov, D. *et al.* Assembly of colloidal semiconductor nanorods in solution by depletion attraction. *Nano Lett.* **10,** 743–749 (2010).
27. Dogic, Z. & Fraden, S. Development of model colloidal liquid crystals and the kinetics of the isotropic–smectic transition. *Phil. Tran. R. Soc. A* **359,** 997–1015 (2001).
28. Hanfland, M., Syassen, K., Christensen, N. E. & Novikov, D. L. New high-pressure phases of lithium. *Nature* **408,** 174–178 (2000).
29. Rabani, E., Reichman, D. R., Geissler, P. L. & Brus, L. E. Drying-mediated self-assembly of nanoparticles. *Nature* **426,** 271–274 (2003).
30. Ozin, G. A., Arsenault, A. C. & Cardemartiri, L. in *Nanochemistry: A Chemical Approach to Nanomaterials* 2nd edn 335–428 (RSC Publishing, 2008).
31. Talapin, D. V., Lee, J-S., Kovalenko, M. V. & Shevchenko, E. V. Prospects of colloidal nanocrystals for electronic and optoelectronic applications. *Chem. Rev.* **110,** 389–458 (2010).
32. Stebe, K. J., Lewandowski, E. & Ghosh, M. Materials science. Oriented assembly of metamaterials. *Science* **325,** 159–160 (2009).
33. Louis, A. A., Bolhuis, P. G., Hansen, J. P. & Meijer, E. J. Can polymer coils be modeled as 'soft colloids'? *Phys. Rev. Lett.* **85,** 2522–2525 (2000).

Acknowledgements

This work was partially supported by the Defense Advanced Research Projects Agency. The shape-selective synthesis part of the work is supported by the Director, Office of Basic Energy Sciences, Materials Sciences and Engineering Division, of the US Department of Energy under contract no DE-AC02-05CH11231. M.G. was supported by the Austrian Science Fund (FWF) under grant no J 3106-N16. M.G. and P.L.G. were supported by the National Science Foundation under grant no CHE-0910981. A.W-C. was supported by the US Department of Energy under contract no DE-AC02-05CH11231. Work at the Molecular Foundry was supported by the Office of Science, Office of Basic Energy Sciences, of the US Department of Energy under contract no DE-AC02-05CH11231. P.Y. thanks the National Science Foundation for the Waterman Award.

Author contributions

J.H. and M.G. both contributed extensively to this work. J.H. initiated the study, conceived and conducted the experiments, analysed results and cowrote the paper. M.G. identified all crystal structures, conceived and implemented the simulations and theoretical models, analysed results and cowrote the paper. A.W-C. suggested simulations and experiments, analysed results, helped prepare figures and cowrote the paper. P.L.G. suggested simulations and experiments, analysed results and cowrote the paper. P.Y. initiated the study, suggested experiments, analysed results and cowrote the paper.

Additional information

The authors declare no competing financial interests. Supplementary information accompanies this paper on www.nature.com/naturematerials. Reprints and permissions information is available online at http://www.nature.com/reprints. Correspondence and requests for materials should be addressed to M.G or P.Y.